Check for updates

Angewandte Chemie International Edition

Angewandte International Edition Chemie

How to cite: *Angew. Chem. Int. Ed.* **2026**, e2426576
doi.org/10.1002/anie.2426576

RESEARCH ARTICLE

Blocked Proton-Coupled Electron Transfer Stabilizes Buried Interface in Air-Processed Inverted Perovskite Solar Cells

Luyao Yan[1] | Zhineng Lan[1] | Yingying Yang[1] | Peng Cui[1] | Fu Yang[1] | Shuxian Du[1] | Shujie Qu[1] | Hao Huang[1] | Meicheng Li[1,2]

[1]State Key Laboratory of Alternate Electrical Power System With Renewable Energy Sources, School of New Energy, North China Electric Power University, Beijing, China | [2]College of Automotive and Energy Engineering, Tongji University, Shanghai, China

Correspondence: Hao Huang (hhuang@ncepu.edu.cn) | Meicheng Li (mcli@ncepu.edu.cn)

Received: 6 June 2026 | **Revised:** 24 August 2026 | **Accepted:** 26 September 2026

Keywords: charge-carrier transport | hole transport layer | interfacial redox reaction | perovskite solar cells | stability

ABSTRACT

Nickel oxide/self-assembled monolayer (NiO_x/SAM) composites have emerged as benchmark hole transport layers for high-efficiency inverted perovskite solar cells (PSCs). However, the coupled interfacial degradation mechanism in NiO_x/SAM/perovskite systems remains ambiguous, which still restricts device stability. In this study, we identify a previously unrecognized proton-coupled electron transfer (PCET) induced buried-interface degradation pathway, in which the protons released from SAM accelerates the redox reaction between NiO_x and I^-, especially under high-temperature and UV-irradiation operation conditions. To block this coupled degradation pathway, we incorporate 1-methylimidazole into the SAM, which suppresses the proton transfer through capturing the protons and impedes the electron transfer through reducing the formation of I^- vacancies, thereby blocking the interfacial PCET process from both perspective of proton and electron. Besides, the proton-capture treatment by 1-methylimidazole can enhance the anchoring of SAM at the NiO_x substrate, which promotes the interface hole transfer and also contributes to the interfacial stability. Consequently, the resulting PSCs, fabricated in ambient air, achieved a power conversion efficiency exceeding 26.3% with an enhanced operational stability by retaining >90% initial efficiency after 2000 h of maximum power point tracking at ~50°C.

1 | Introduction

Inverted perovskite solar cells (p-i-n PSCs) are at the forefront of technological development due to their distinct advantages, including low-temperature fabrication feasibility, superior compatibility with flexible substrates and tandem architectures [1, 2]. Recent progress in hole transport layers (HTL) play a vital role in enabling the certified power conversion efficiencies (PCE) exceeding 27.0% for p-i-n PSCs [3, 4]. Among various HTL systems, nickel oxide/self-assembled monolayer (NiO_x/SAM) composites have become the benchmark system for high-efficiency p-i-n PSCs [5]. The NiO_x layer provides a favorable substrate and effective hole extraction capability, while SAM molecules represented by Me-4PACz further reduce contact losses through interface modification, jointly achieving efficient interface hole transport [6–8]. However, due to the intrinsic reactivity of the NiO_x surface, deprotonation and desorption of SAM molecules, the interfacial stability remains a key bottleneck currently limiting PSCs performance and practical applications [9–12].

With regard to the HTL interfacial stability, extensive research has been carried out on NiO_x and SAM modification, respectively. As a typical metal oxide, NiO_x possesses highly active Ni species on its surface, which can trigger redox reactions with lead-iodide species in perovskite [13–15]. These reactions cause deprotonation

All rights reserved, including rights for text and data mining and training of artificial intelligence technologies or similar technologies.
© 2026 Wiley-VCH GmbH

of A-site cations and oxidation of X-site ions in perovskite, accompanied by severe interfacial non-radiative recombination. To address these issues, surface modification strategies such as reductant introduction, as well as doping engineering, have been adopted to passivate reactive Ni sites and suppress interfacial degradation. In terms of SAMs, their interfacial instability mainly originates from the deprotonation and desorption of acidic terminal groups (e.g., phosphonic acid and carboxylic acid groups), as well as chemical reactions with perovskite components [16, 17]. These behaviors lead to SAM layer failure and oxidation of perovskite lead-iodide species. Current studies primarily focus on screening chemically stable SAM molecular structures via electron-withdrawing group introduction and steric hindrance enhancement, or optimizing weakly acidic terminal groups to strengthen molecular anchoring and reduce interfacial reactivity [7, 18, 19].

Nevertheless, in practical applications of NiO_x/SAM composite HTL systems, the interfacial reactions induced by NiO_x and SAM are mutually coupled and synergistic [15, 20, 21]. The SAM molecules not only react with the perovskite components, but also their adsorption behavior is affected by the oxidation state of the NiO_x surface. This synergistic interplay complicates the interfacial chemical reaction and may further accelerate interfacial degradation [22, 23]. Previous studies have identified several important degradation pathways at inverted buried interfaces, including redox reactions between high-valence Ni species and iodide species, defect generation induced by reactive NiO_x surfaces, SAM deprotonation or desorption, and insufficient molecular anchoring [10, 15, 16, 20–24]. These studies have greatly advanced the understanding of buried-interface instability; however, most of them focused on one dominant interfacial factor, either NiO_x-related redox chemistry or SAM-related anchoring instability. Therefore, it is urgent to explore the interfacial reaction mechanism and develop corresponding suppression strategies by considering the combined effects of NiO_x and SAM, so as to enhance PSCs interfacial stability [25].

Herein, we comprehensively consider the coupled effects among NiO_x, SAM, and perovskite components and explore the key chemical reaction mechanisms underlying interfacial degradation of p-i-n PSCs. We reveal that the protons released from Me-4PACz accelerate iodide-to-NiOx electron transfer through a proton-coupled electron transfer (PCET) process, thereby inducing severe interfacial degradation. This PCET process becomes more pronounced under UV illumination and high temperature. To address this, we introduced 1-methylimidazole (NMI) into the Me-4PACz precursor solution as a proton capturer. The pyridinic nitrogen in NMI with its lone pair electrons effectively captures protons, which inhibits the proton participation in the interfacial reaction. Besides, the NMI can also suppress the formation of V_I, which impedes the electron transfer from the I^- to high-valence Ni^{3+} species. These dual effects, involving both proton capture and electron-transfer suppression, jointly block the PCET process, thus preventing interfacial reactions. This approach reduces the interfacial defect density, improves interfacial carrier transport, and enhances interfacial stability. As a result, we fabricated PSCs in ambient air that achieved a PCE exceeding 26.3%. The NMI-based PSCs maintained 87% of their initial efficiency after being aged under UV irradiation for 1200 h, while the PSCs without NMI decreased to 68%. Moreover, the NMI-based PSCs retained over 90% of their initial efficiency after 2000 h of maximum power point tracking at ~50°C, demonstrating remarkable operational stability.

2 | Results and Discussion

2.1 | Interface Chemical Reaction Mechanism

Previous studies have extensively investigated the reactions between NiO_x and perovskite components, primarily focusing on the redox reaction between high-valent Ni and perovskite components [26, 27]. To explore the SAM-participated coupled interfacial reactions, Me-4PACz was introduced into the reaction system of NiO_x and perovskite components in this work, aiming to clarify the influence of SAM on interfacial reaction behaviors. We prepared a mixed solution of NiO_x and FAI for UV–vis absorption measurements. As shown in Figure 1a, a notable absorption peak corresponding to I_3^- emerged at approximately 350 nm, indicating the formation of I_2 considering that the I_2 can combine with I^- to form I_3^-, which demonstrates the redox reaction between NiO_x with I^- [16]. The introduction of Me-4PACz into the NiO_x/FAI mixed solution significantly increased the intensity of the I_3^-absorption peak, indicating that Me-4PACz accelerates the oxidation of I^-. Upon UV irradiation, the I_3^-absorption intensity was further enhanced, and a distinct color change was also observed in Me-4PACz, NiO_x, and FAI mixture solution. Furthermore, the mixture solution of Me-4PACz, NiO_x, and FAI was continuously heated at 65°C to track the evolution of the I_3^-absorption peak (Figure 1b). The I_3^-absorption intensity increases continuously as the heating time prolonged. These results indicate that the participation of Me-4PACz accelerates the NiO_x/FAI redox reaction, and such reaction among them can be further intensified under UV irradiation and high temperature.

To further visualize the accelerated redox reaction between NiO_x and FAI induced by Me-4PACz, we used conventional three-electrode cyclic voltammetry (CV) measurements to analyze the chemical reactions involving NiO_x, Me-4PACz, and FAI at the buried interface. During the testing process, we deposited NiO_x on the carbon cloth to serve as the working electrode, and added FAI and Me-4PACz to the electrolyte solution. As shown in Figure 1c, compared with the electrolyte without Me-4PACz addition, there is a more obvious Ni^{3+}/Ni^{2+} ion pair reduction peak near ~0.25 V as well as oxidation peaks of I^-/I_3^- and I_3^-/I^0 ion pairs at higher potentials. This means that Me-4PACz will simultaneously accelerate the reduction process of Ni^{3+}/Ni^{2+} as well as the oxidation processes of I^-/I_3^- and I_3^-/I^0.

Given that Me-4PACz contains strongly acidic phosphonic acid groups, we speculate that it is the H^+ released by Me-4PACz that accelerates the redox reaction [16]. This interfacial redox interaction between I^- and NiO_x, mediated by H^+, proceeds via a PCET mechanism [28]. Consequently, Me-4PACz expedites interfacial degradation through a PCET process (Figure 1d). Specifically, I^- donate electrons, while Me-4PACz undergoes deprotonation. Both electrons and protons are transferred synchronously to NiO_x: the electrons reduce Ni^{3+} to Ni^{2+}, and the protons migrate toward lattice oxygen (forming Ni–OH from Ni–O). This leads to the reduction of Ni^{3+} and leaves a significant number of V_I at the buried interface. The proposed mechanism for the interface PCET

15213773, 0, Downloaded from https://onlinelibrary.wiley.com/doi/10.1002/anie.202526576 by North China Electric Power University Beijing, Wiley Online Library on [08/10/2026]. See the Terms and Conditions (https://onlinelibrary.wiley.com/terms-and-conditions) on Wiley Online Library for rules of use; OA articles are governed by the applicable Creative Commons License

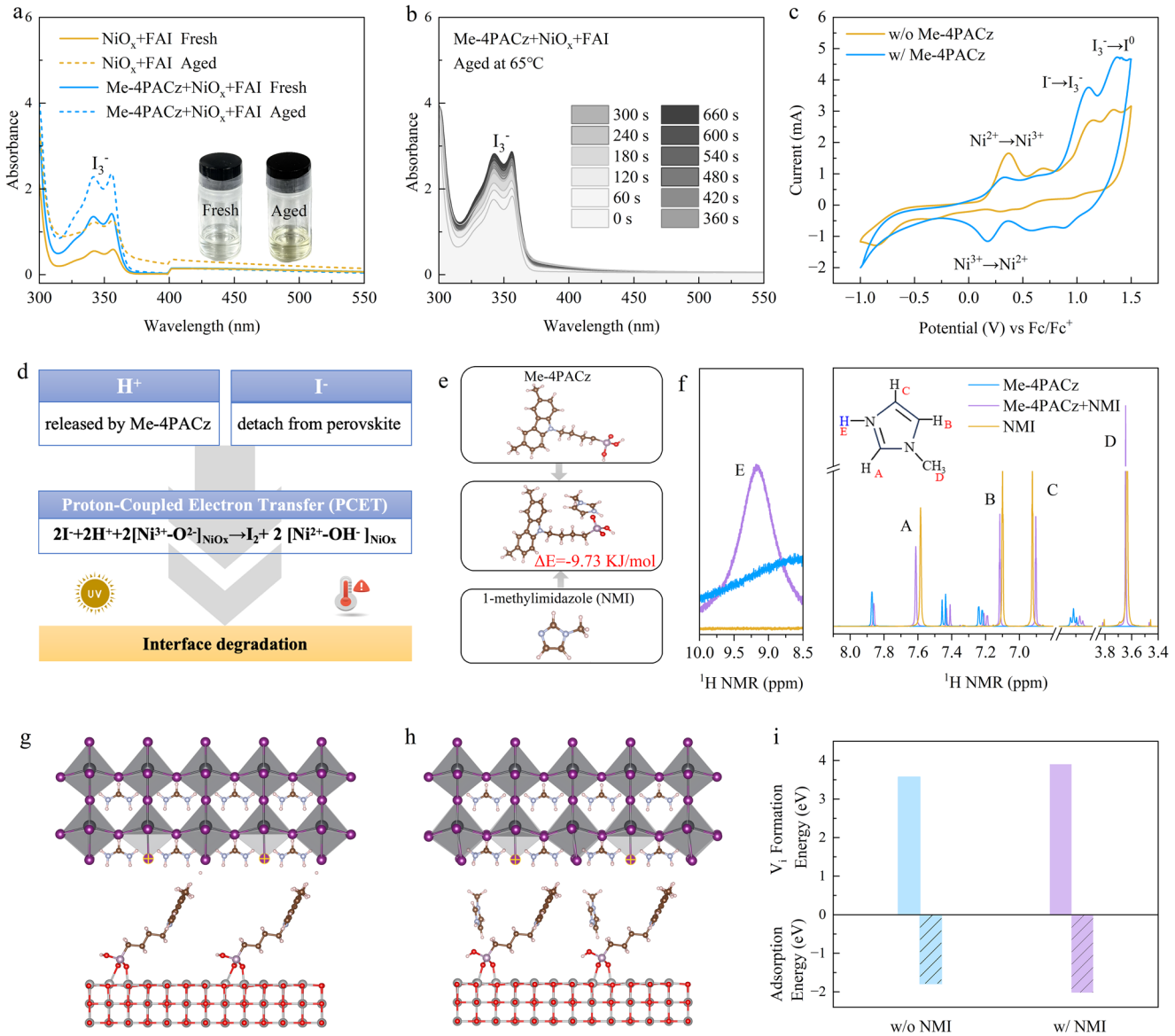


FIGURE 1 | Interface chemical reaction mechanism. (a) The UV–vis spectra of mixture solution before and after UV aging. The inset is a photograph of the Me-4PACz, NiO_x, and FAI mixture solution before and after UV aging. (b) The in situ UV–vis spectra of mixture solution under 65°C aging. (c) Cyclic voltammetry of NiO_x deposited on a hydrophilic carbon cloth electrode in an electrolyte solution containing FAI, or Me-4PACz. (d) Schematic degradation of interface caused by the PCET process. (e) The binding energy changes of NMI with Me-4PACz. (f) 1H NMR spectra of NMI, Me-4PACz, and Me-4PACz with NMI. (g, h) Lattice models without and with NMI used for calculating the formation energy of V_I. (i) V_I formation energy and the adsorption energy of Me-4PACz on NiO_x.

among I^-, Me-4PACz, and NiO_x is summarized as follows:

$$2I^- + 2H^+ + 2[Ni^{3+} - O^{2-}] \rightarrow I_2 + 2[Ni^{2+} - OH^-]$$

The regulation of PCET process faces significant challenges, as it is simultaneously constrained by both the electronic driving force and the protonation energy [29]. After carefully examining the relevant literature, we note that although PCET is a well-established chemical concept, its reported use in PSCs has mainly focused on beneficial molecular processes, such as PCET-mediated Spiro-OMeTAD doping in conventional devices [30]. In contrast, the role of PCET as a buried-interface degradation pathway in NiO_x/SAM-based inverted PSCs remains largely unexplored. Considering the mutual coupling relationship between electrons and protons in PCET, blocking PCET not only requires capturing protons and inhibiting their participation in the reaction, but also requires anchoring I^- to impede the transfer of electrons from I^- to high-reactive Ni^{3+} species. Based on this, we employ NMI (chemical structure shown in Figure S1), which possesses proton-capturing capability, to pre-capture protons released by SAM; simultaneously, impede transfer of electron from free I^-, since the pyridine nitrogen in NMI has been reported to interact with perovskite and inhibit the formation of free I^- [31]. In addition, the capture of protons can also enhance the anchoring stability of Me-4PACz on the NiO_x substrate, thereby physically blocking the direct contact between NiO_x and the I^-.

15213773, 0, Downloaded from https://onlinelibrary.wiley.com/doi/10.1002/anie.202526576 by North China Electric Power University Beijing, Wiley Online Library on [08/10/2026]. See the Terms and Conditions (https://onlinelibrary.wiley.com/terms-and-conditions) on Wiley Online Library for rules of use; OA articles are governed by the applicable Creative Commons License

These impede from both transfer of proton and electron jointly blocks the PCET process, thus preventing interfacial degradation reactions.

During the proton capture process, NMI combines with the labile hydrogen on the phosphonic acid group of Me-4PACz. We employed density functional theory (DFT) to analyze the structural energy changes in this bound state to confirm the feasibility of proton capture from Me-4PACz by NMI. Initially, we randomly generated 200 structural configurations each for two states: the S_0 state, where NMI and Me-4PACz exist independently without binding, and the S_1 state, where a proton is transferred from Me-4PACz to NMI. After two rounds of screening and optimization, the lowest-energy S_0 and S_1 configurations were obtained (Figures 1e and S2). The energy comparison between the two states (Es_1-Es_0 = −9.73 kJ/mol) confirmed that Me-4PACz preferentially transfers its proton to the pyridinic nitrogen of NMI.

Furthermore, we utilized NMR to confirm the proton capture by NMI, resulting in the formation of $NMIH^+$. NMI is a five-membered heteroaromatic ring containing two nitrogen atoms: N1 is substituted with a methyl group (—CH_3), while N3 is an unsubstituted nitrogen. The ring hydrogens can be classified into three types: A–H (located between the two nitrogen atoms), B–H/C–H (the other two ring C—H bonds), and methyl hydrogens (—CH_3). In the imidazole ring, the lone pair on N3 is not involved in conjugation (the lone pair on N1 participates in conjugation to maintain aromaticity), so protonation preferentially occurs at N3, generating $NMIH^+$ (where N3 bears a positive charge). As shown in Figure 1f, after protonation to form $NMIH^+$, all hydrogen signals except that of C—H, which forms a hydrogen bond with the phosphonate group of Me-4PACZ, shift downfield (increase in δ). A–H experiences a strong downfield shift due to the combined electron-withdrawing inductive effects of the two adjacent nitrogen atoms and reduced shielding from the heteroaromatic ring. B–H, separated from N3 by one carbon atom, shows a smaller downfield shift due to attenuation of the inductive effect through chemical bonds. In contrast, C—H forms a weak hydrogen bond with an oxygen atom on the phosphonate group; the lone pair on oxygen provides slight electron density feedback to C—H via hydrogen bonding, increasing electron density around C–H and thus shifting its signal up field (decrease in δ). For the Me-4PACz with NMI sample, a weak signal appears near 9.1 ppm, which corresponds to the N3–H signal after rapid proton capture by NMI from the labile hydrogen on the phosphonic acid group of SAM. This confirms the proton-capturing ability of NMI.

The x-ray photoelectron spectroscopy (XPS) N1s spectra of the FTO/NiO_x/Me-4PACz film with and without NMI, as well as that of the NMI molecule itself, are shown in Figure S3. The N1s spectra of NMI can be deconvoluted into two peaks corresponding to the pyridinic nitrogen and the pyrrolic nitrogen. The pyridinic nitrogen, possessing a lone pair of electrons, can accept a proton. Consequently, in the FTO/NiO_x/Me-4PACz film with added NMI, the pyridinic nitrogen signal shifts toward a higher binding energy, confirming the capture of labile protons from Me-4PACz by NMI. Therefore, the P 2p signal of Me-4PACz in the film with NMI also shifts to a higher binding energy (Figure S4). These results further confirm that NMI captures the protons of Me-4PACz.

As discussed, NMI inhibit the formation of free I^- to impede electron transfer, and after the protons are captured, the anchoring ability of Me-4PACz will be enhanced. So, we performed DFT calculations on the V_I formation energy at the perovskite buried interface (Figure 1g,h) and the binding energy of Me-4PACz molecules adsorbed on NiO_x (Figure S5). As shown in Figure 1i, the introduction of NMI increased the V_I formation energy from 3.574 to 3.904 eV at the perovskite buried interface deposited on NMI-modified Me-4PACz. Concurrently, the binding energy of Me-4PACz on NiO_x decreased from −1.795 to −2.014 eV. The above researches have shown that NMI can capture protons and inhibit the formation of V_I, and coupled the enhanced anchoring ability of Me-4PACz. These impede from both transfer of proton and electron jointly, thereby is expected to block the interface PCET process.

2.2 | Interfacial Property Optimization

To visually verify the inhibition of NMI on the interface reaction, we conducted UV–vis tests on the mixed solutions of NiO_x, Me-4PACz, FAI, and NMI. Compared with the distinct color change of the mixture solution and the enhancement of the I_3^- signal peak observed in UV–vis spectra (Figure 1a,b), the solution with NMI exhibited remarkable stability throughout the UV irradiation, as shown in Figure 2a. Furthermore, under continuous heating conditions, no significant change in the intensity of I_3^- was observed (Figure 2b). These UV–vis spectra indicated that NMI inhibited the oxidation of I^- in the redox reaction involving NiO_x, Me-4PACz, and FAI. The same effect of NMI in blocking PCET was also observed in the CV measurement (Figure S6). The incorporation of NMI into the electrolyte leads to a slight decrease in the reduction potential of Ni^{3+}/Ni^{2+} and an increase in the oxidation potential of I^-/I_3^- and I_3^-/I^0, signifying a higher energy demand for the initiation of redox reactions [26]. Consequently, the introduction of NMI at the interface will consume protons at the interface, causing the reduction potential of Ni^{3+}/Ni^{2+} to shift negatively, thereby reducing the reactivity of the PCET reaction.

XPS Ni 2p spectra were employed to investigate the influence of blocking PCET on the chemical states of NiO_x thin films. We fabricated the sample with the structure of FTO/NiO_x/Me-4PACz/perovskite and carried out ultraviolet aging treatment. Then we removed the perovskite film before the test to enable a true observation of the effect of PCET on the chemical states of NiO_x. The signal peaks corresponding to Ni^{3+} and Ni^{2+} species in the Ni $2p_{3/2}$ spectra are labeled in Figure 2c,d, respectively [32]. Notably, Ni^{2+} serves as the fundamental valence state of NiO_x, which contains no additional holes and contributes to a stable lattice structure. Ni^{3+} can be considered as the product of electron loss from Ni^{2+}; each Ni^{3+} formed leaves one hole in the lattice, representing the primary source of holes in NiO_x and thus determining the carrier concentration. After the introduction of NMI, the Ni^{3+}/Ni^{2+} area ratio increases from 2.24 to 2.56. This phenomenon suggests that proton capture by NMI is beneficial for blocking the PCET at the interface, thereby balancing the valence states of NiO_x and enhancing its hole transport capability.

In order to clarify the impact of blocking PCET at the HTL/perovskite interface on the stability of interface charge-carrier transport, we prepared complete PSCs with the structure

15213773, 0, Downloaded from https://onlinelibrary.wiley.com/doi/10.1002/anie.202526576 by North China Electric Power University Beijing, Wiley Online Library on [08/10/2026]. See the Terms and Conditions (https://onlinelibrary.wiley.com/terms-and-conditions) on Wiley Online Library for rules of use; OA articles are governed by the applicable Creative Commons License

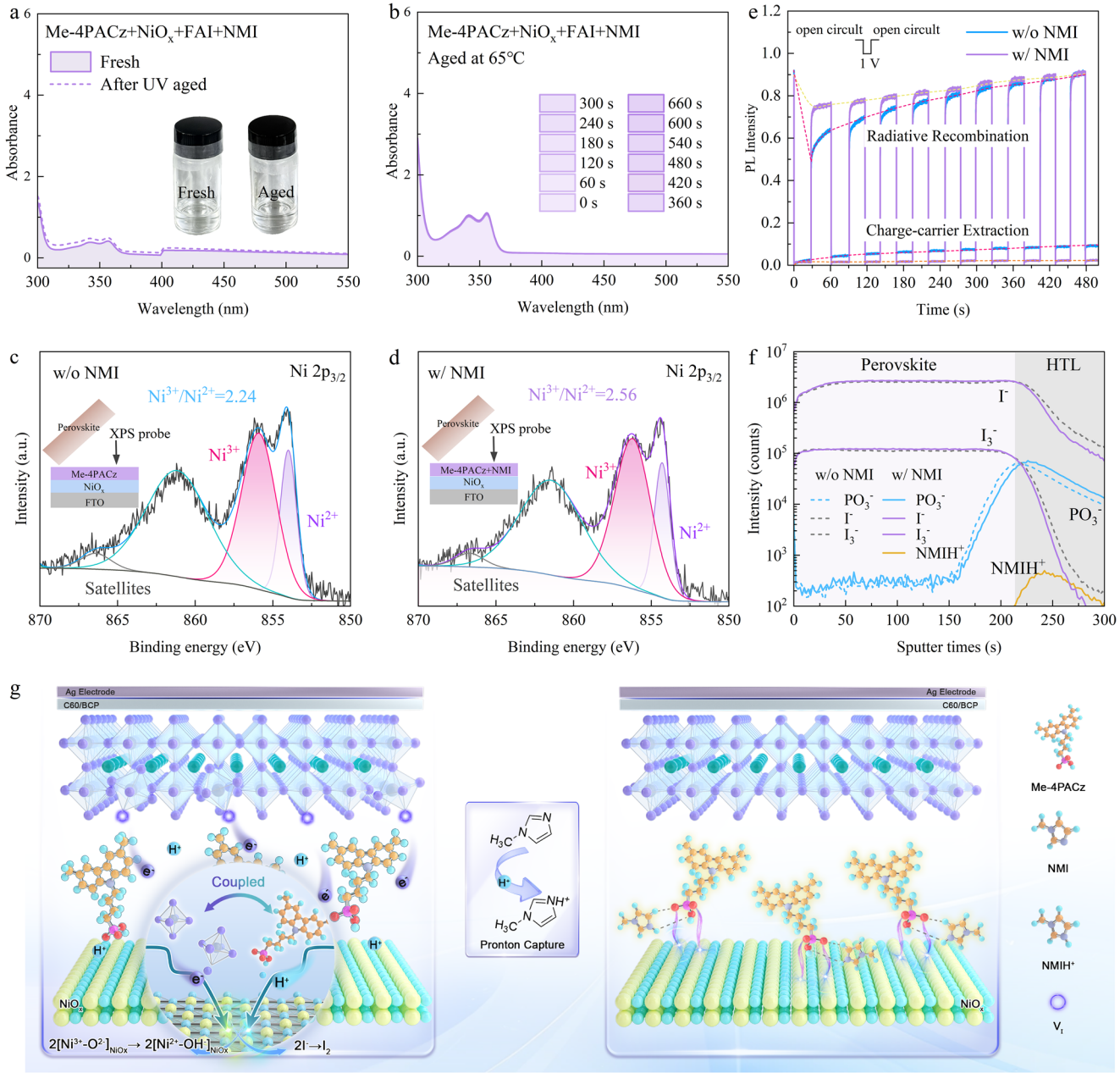


FIGURE 2 | Interfacial property optimization. (a) The UV–vis spectra of mixture solution. The inset is a photograph of the Me-4PACz, NiO_x, FAI, and NMI mixture solution before and after UV aging. (b) The in situ UV–vis spectra of mixture solution under 65°C aging. (c, d) XPS spectra of Ni $2p_{3/2}$ of NiO_x/Me-4PACz and NMI-based NiO_x/Me-4PACz. (e) The PL evolution of PSCs under open circuit/1 V/open circuit cycle. (f) ToF-SIMS elemental depth profiles of FTO/NiO_x/Me-4PACz/perovskite without and with NMI. (g) Mechanism schematic diagram of PCET and PCET blocked by NMI.

of FTO/NiO_x/Me-4PACz/perovskite/C_{60}/BCP/Ag. Then, examined the evolution of photoluminescence (PL) in PSCs under an open circuit/1 V bias/open circuit cycling. Under open-circuit conditions, the PSCs exhibited high PL intensity through radiative recombination. Upon application of a 1 V bias, which facilitates charge carrier separation and extraction, the PL intensity decreased rapidly, indicating efficient extraction of carriers. As shown in Figure 2e, in the first cycle, the PSCs undergoes the application of bias voltage to accelerate carrier separation, followed by the withdrawal 1 V bias, and the PSCs recovers its PL intensity [33, 34]. The significant contrast is that the NMI based PSCs can rapidly recover to 81% of the initial PL intensity and then stabilize at 85% of the initial intensity, while PSCs without NMI only recover to 53% of the initial intensity and then slowly recover to 65%. After 10 cycles, under the condition of applying 1 V bias, the carrier separation degree of NMI-based PSCs was high, and the PL intensity decay was also significant. However, the PL intensity of PSCs without NMI kept increasing, indicating that the charge-carrier separation at the interface was hindered. These results demonstrated that the introduction of NMI can enhance the stability of the interface and ensure that the carriers at the interface can be separated stably and completely. Time-of-flight secondary ion mass spectrometry (ToF-SIMS) was further employed to investigate the chemical environment at the HTL/perovskite interface. As shown in Figure 2f, I^- at the perovskite bottom interface exhibited a tendency to migrate

15213773, 0, Downloaded from https://onlinelibrary.wiley.com/doi/10.1002/anie.202505676 by North China Electric Power University Beijing, Wiley Online Library on [08/10/2026]. See the Terms and Conditions (https://onlinelibrary.wiley.com/terms-and-conditions) on Wiley Online Library for rules of use; OA articles are governed by the applicable Creative Commons License

toward the HTL layer, accompanied by increased generation of I_3^- species. Furthermore, some insufficiently anchored Me-4PACz molecules migrated into the perovskite layer. These phenomena were significantly mitigated after the addition of NMI. The capture of free H^+ by NMI can inhibit the migration of I^- at the buried interface of perovskite and enhance the anchoring ability of phosphonate groups on the surface of NiO_x [17]. Therefore, proton capture by NMI contributes to the stability of the chemical environment at the HTL/perovskite interface, which serves as a critical prerequisite for the improvement of interfacial charge-carrier transport.

We summarized and described the PCET mechanism at HTL/perovskite interface (Figure 2g). At the buried interface of p-i-n PSCs, the H^+ released by Me-4PACz promotes the detachment of I^- from the perovskite lattice. Meanwhile, owing to the weak binding and incomplete coverage of Me-4PACz on NiO_x, Ni^{3+} become more accessible to I^-, thereby accelerating the redox reaction between them. NMI can pre-capture the H^+ released by Me-4PACz, prevent free I^- from providing electrons, and enable the phosphonate groups to better anchor on the surface of NiO_x, suppressing the PCET process at the HTL/perovskite interface.

2.3 | Improvement of Interface Charge-Carrier Transport

We then investigated the influence of NMI on interfacial charge-carrier dynamics. First, we characterized the morphology of the perovskite buried interface. When depositing perovskite films on FTO/NiO_x/Me-4PACz, the chemical properties of the substrate inevitably influence the nucleation and growth of the perovskite [21, 35, 36]. As shown in the cross-sectional SEM image in Figure 3a, the Me-4PACz without NMI containing a large number of unanchored phosphonic acid groups, which react with the perovskite, resulting in numerous voids in the cross-section [16]. In contrast, the perovskite film deposited with NMI exhibited good contact with the FTO/NiO_x/Me-4PACz substrate. By peeling off the perovskite film to examine the surface morphology of the buried interface, we observed that the film deposited on Me-4PACz without NMI contained a significant amount of PbI_2 residue at the grain boundaries (Figure 3b). This is likely due to the decomposition of the perovskite following the formation of V_I. The presence of extensive PbI_2 residue at the grain boundaries can adversely affect carrier generation and transport [36]. In comparison, the perovskite film deposited on Me-4PACz with NMI displayed noticeably larger and more uniform grain sizes (Figure 3c). XPS spectra of Pb 4f observed that the introduction of NMI reduced the content of Pb^0 at the buried interface of perovskite film (Figure S7), which indicates that the interface quality has been improved.

Furthermore, we investigated the improvement of the photoelectric properties of the obtained FTO/NiO_x/Me-4PACz films. After the introduction of NMI, the film conductivity increased from 3.5×10^{-3} S/cm to 9.5×10^{-3} S/cm (Figure 3d). We also characterized that hole mobility increased from 5.35×10^{-4} cm^2/V s to 3.93×10^{-3} cm^2/V s (Figure 3e). The improved conductivity and hole mobility should result from that NMI captures the protons released by Me-4PACz, which is beneficial for enhancing the anchoring ability and coverage uniformity on the surface of NiO_x. Ultraviolet photoelectron spectroscopy (UPS) was employed to investigate the influence of NMI on the interfacial energy level structure. After calculating the valence band maximum (VBM) of different HTL, we reveal that NMI shifts the VBM downward of NiO_x/Me-4PACz from −5.36 to −5.63 eV, minimizing the energy barrier for hole extraction (Figure 3f,g). This improved alignment with NMI incorporation is expected to enhance hole transfer efficiency and reduce interfacial recombination.

The carrier transport capability of the HTL was further investigated by steady-state PL, time-resolved PL (TRPL), transient photocurrent (TPC), and transient photovoltage (TPV). The PL spectrum of FTO/NiO_x/NMI-Me-4PACz/perovskite exhibit an obvious intensity quenching (Figure S8). TRPL results are shown in Figure 3h, and Table S1, the τ_1 of FTO/NiO_x/NMI-Me-4PACz/perovskite is 388.8 ns, which is smaller than that (503.6 ns) of without NMI. These results indicate that blocking PCET can suppress interface defects and charge accumulation. The promoted interface charge transport was also validated by the TPC results, where the TPC decay lifetime of the PSCs with NMI (2.3 μs) is shorter than that (6.2 μs) of the PSCs without NMI (Figure S9). As for the TPV test, the lifetime of PSCs with NMI is 7.2 μs, much longer than that of the PSCs without NMI (1.4 μs), indicating the suppressed interfacial carrier recombination (Figure 3i). These results collectively verify that proton capture by NMI inhibit non-radiative recombination, and accelerates charge transport kinetics.

2.4 | Photovoltaic Performance

We fabricated twenty PSCs with NMI and twenty without in ambient air. The PSCs had a structure of FTO/NiO_x/Me-4PACz/Perovskite/C_{60}/BCP/Ag and an active area of 0.08 cm^2. The *J–V* curves of the champion PSCs are presented in Figure 4a. The NMI-based PSCs reached a PCE of 26.3%, with a J_{SC} of 26.2 mA cm^{-2}, a V_{OC} of 1.19 V, and an FF of 84.4%, while the PSCs without NMI achieved a PCE of 25.3%, with a J_{SC} of 26.0 mA cm^{-2}, a V_{OC} of 1.17 V, and an FF of 83.0%. The NMI-based PSCs also exhibited lower hysteresis. The PCE distribution confirms that introducing NMI to capture protons and suppress PCET effectively enhances PSCs' performance (Figures 4b and S10). The corresponding external quantum efficiency (EQE) spectrum (Figure S11) gave an integrated J_{SC} of 25.7 mA cm^{-2} for the NMI-based PSCs. Under a bias of 1.03 V over 300 s, the steady-state power output measurement (Figure 4c) indicated the NMI-based PSCs had relatively stable output power, which was attributed to the enhancement in interface quality. The correlation between V_{OC} and illumination intensity was analyzed based on the relation $V_{OC} = (n_{ID}kBT/q)\ \ln(I)$, where k_B denotes the Boltzmann constant and q represents the elementary charge. The calculated ideality factors (n_{ID}) were 2.23 and 1.34 for PSCs without and with NMI addition, respectively (Figure 4d). A smaller n_{ID} value suggests suppression of trap-assisted recombination in the devices, which aligns with the space-charge-limited current (SCLC) measurements and dark *J–V* analyses (Figures 4e and S12). These results demonstrate that high-quality interfaces between HTL and perovskite can effectively mitigate non-radiative charge recombination, thereby contributing to enhanced device performance.

15213773, 0, Downloaded from https://onlinelibrary.wiley.com/doi/10.1002/anie.202526576 by North China Electric Power University Beijing, Wiley Online Library on [08/10/2026]. See the Terms and Conditions (https://onlinelibrary.wiley.com/terms-and-conditions) on Wiley Online Library for rules of use; OA articles are governed by the applicable Creative Commons License

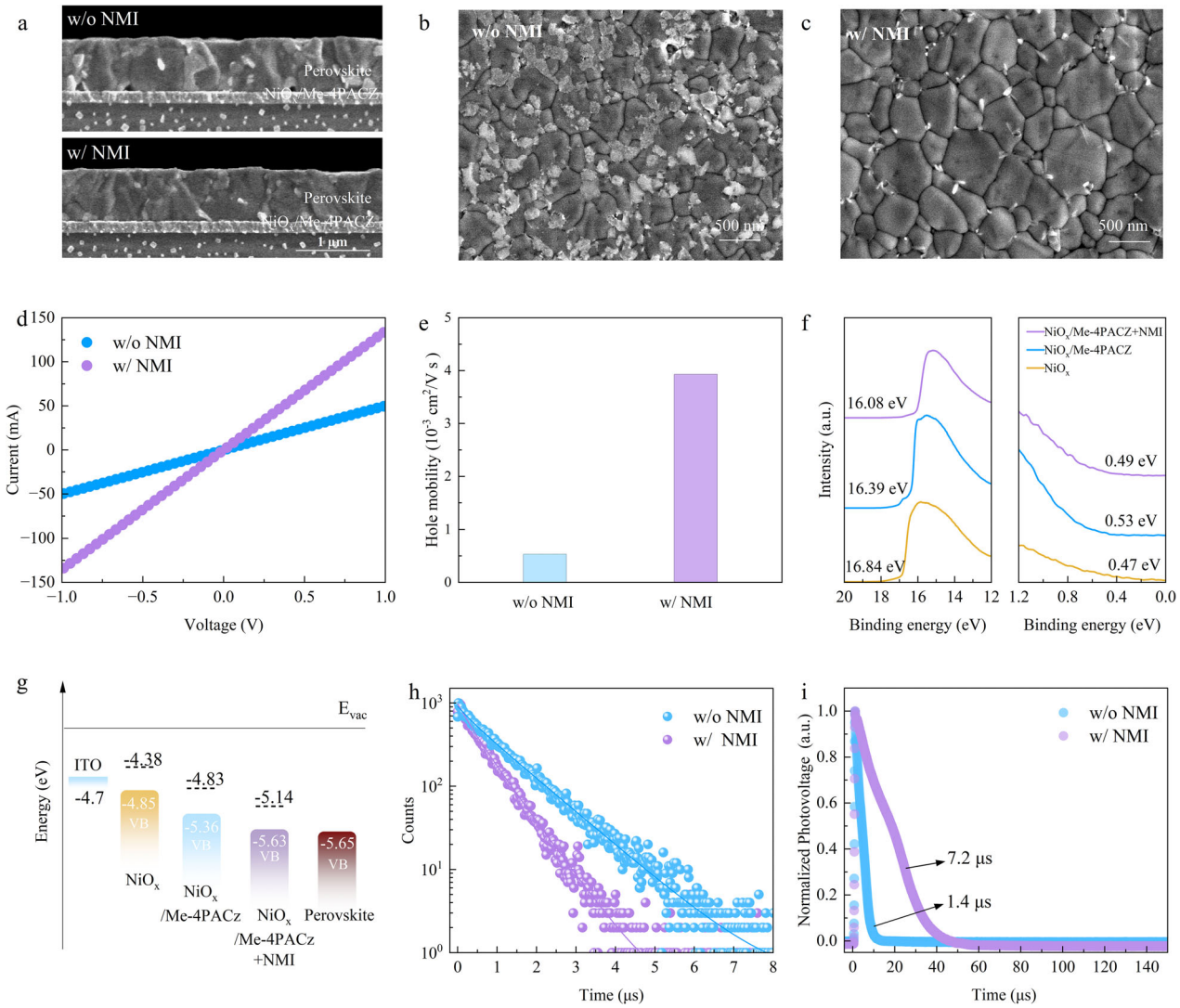


FIGURE 3 | Characterization of interface carrier transport. (a) Cross-sectional SEM image of FTO/NiO_x/Me-4PACz/perovskite. (b, c) The SEM image of perovskite buried interface deposited on FTO/NiO_x/Me-4PACz. (d, e) Conductivity and Hall measurements of NiO_x/Me-4PACz. (f, g) UPS spectra and the corresponding energy-level diagram. (h, i) TRPL and TPV results of FTO/NiO_x/Me-4PACz/perovskite.

The desorption of SAM may lead to inconsistent spatial current distribution, which prevents effective electron-blocking and ultimately results in PSCs breakdown under reverse bias. Therefore, the reverse breakdown voltage of the cell can serve as an initial indicator of reliability improvement associated with enhanced HTL quality [33, 34]. As shown in Figure 4f, the breakdown voltage increases to −6.4 V for the NMI-based PSCs, indicating improved SAM anchoring after NMI modification. This more stable SAM effectively blocks electron injection and prevents PSCs breakdown under reverse bias. We also investigated the PCE evolution of unencapsulated PSCs under different accelerated aging conditions. First, considering the accelerating effect of UV irradiation on the PCET process at the PSCs interface, we exposed the unencapsulated PSCs to long-term UV irradiation and monitored the PCE decay. As shown in Figure 4g, after 1200 h of continuous UV irradiation, the PCE of NMI-based PSCs maintained 87%, while the PCE of the PSCs without NMI decreased to 68% of the initial efficiency. This indicates that the excellent interface quality of the PSCs can resist ultraviolet aging, and exhibit better stability during long-term operation.

We further measured the long-term operational stability of the unencapsulated PSCs under continuous illumination (AM1.5G, ~50°C) using MPP tracking systems in a N_2 filled glovebox. As shown in Figure 4h, the PCE of the PSCs without NMI exhibited rapid degradation within the first 200 h, while PSCs with NMI maintained 90% of their initial PCE (T_{90}) after nearly 2000 h. This demonstrates that the strategy of blocking PCET substantially enhances photothermal stability under realistic and accelerated test conditions.

3 | Conclusion

We investigated the chemical reaction mechanism at the HTL/perovskite interface in p-i-n PSCs, discovering the protons released by Me-4PACz accelerate the redox reaction at the interface through PCET process. We proposed a strategy of using NMI to capture protons, inhibit the formation of V_I, and simultaneously impede the transfer of protons and electrons, thereby blocking PCET at the HTL/perovskite interface and

15213773, 0, Downloaded from https://onlinelibrary.wiley.com/doi/10.1002/anie.202526576 by North China Electric Power University Beijing, Wiley Online Library on [08/10/2026]. See the Terms and Conditions (https://onlinelibrary.wiley.com/terms-and-conditions) on Wiley Online Library for rules of use; OA articles are governed by the applicable Creative Commons License

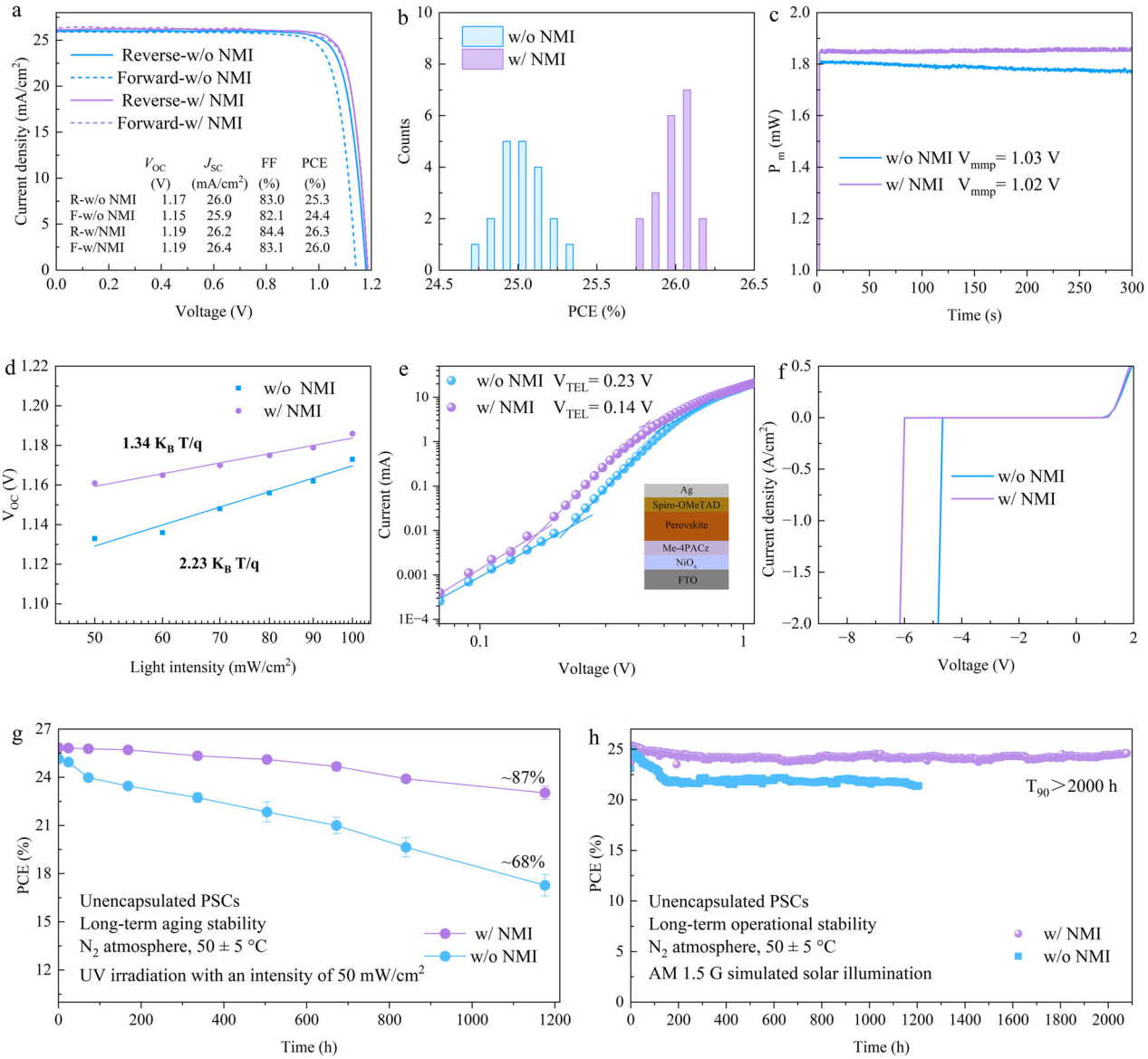


FIGURE 4 | Photovoltaic performance characterization. (a) *J--V* curves of PSCs without and with NMI. (b) Distribution histograms of the PCE values. (c) The steady-state power output of PSCs. (d) V_{OC} of PSCs plotted against the logarithm of light intensity. (e) The SCLC results of HTL-only devices. (f) The breakdown voltage of PSCs. (g) The PCE evolution of unencapsulated PSCs aged under UV irradiation. (h) Light-soaking stability of unencapsulated PSCs under the illumination of AM1.5G.

enhancing the stability of the interface charge-carrier transport. As a result, the PCE of p-i-n PSCs incorporating NMI fabricated in ambient air was increased to 26.3%, and the T_{90} operational lifetime of the PSCs was improved to 2000 h. The interface reaction mechanism and inhibition strategy revealed in this work are expected to provide theoretical guidance and support for enhancing the operational stability of PSCs, promoting their industrial application.

Author Contributions

Luyao Yan: conceptualization, investigation, funding acquisition, writing – original draft, methodology, validation, visualization, writing – review and editing, formal analysis, project administration, resources, data curation, software. **Zhineng Lan:** conceptualization, investigation. **Yingying Yang:** data curation, formal analysis, validation, supervision. **Peng Cui:** supervision, funding acquisition, project administration. **Fu Yang:** methodology, software. **Shuxian Du:** methodology. **Shujie Qu:** methodology. **Hao Huang:** conceptualization, writing – original draft, funding acquisition, writing – review and editing, data curation. **Meicheng Li:** conceptualization, supervision, funding acquisition, project administration, data curation, resources.

Acknowledgments

This work is supported partially by the National Natural Science Foundation of China (Grant Nos. 52232008, 52502251, 52102245, 52402254, and 22409061), the Beijing Natural Science Foundation (Grant Nos. 26JL001 and Z240024), the Key Research and Development Program sponsored by the Ministry of Science and Technology (MOST) (Grant No. 2022YFB4200301), the project of China Three Gorges Corporation named key technologies of intelligent joint regulation and operation with grid connected friendly in power station group of wind, solar photovoltaic and energy storage (Grant No. WWKY-2021-0173), Huaneng Group Headquarters Science and Technology Project (HNKJ20-H88),

15213773, 0, Downloaded from https://onlinelibrary.wiley.com/doi/10.1002/anie.202526576 by North China Electric Power University Beijing, Wiley Online Library on [08/10/2026]. See the Terms and Conditions (https://onlinelibrary.wiley.com/terms-and-conditions) on Wiley Online Library for rules of use; OA articles are governed by the applicable Creative Commons License

the Fundamental Research Funds for the Central Universities (Grant Nos. 2024MS036 and 2025MS038), the Postdoctoral Fellowship Program of CPSF under Grant No. GZB20250045, and the NCEPU "Double First-Class" Program.

Conflicts of Interest

The authors declare no conflicts of interest.

Data Availability Statement

The data that supports the findings of this study are available in the Supporting Information of this article.

References

1. L. Zhao, Z. Chu, S. Yang, et al., "Homogeneously Distributed Self-Assembled Molecules for Efficient and Scalable Perovskite/Silicon Tandem Solar Cells," *Joule* (2026): 102492, https://doi.org/10.1016/j.joule.2026.102492.

2. T. Miao, S. Liu, X. Lei, et al., "An Entropy-Regulating Molecular Lock Stabilizes Formamidinium Lead Halide Perovskite," *Science* 392 (2026): 742–748, https://doi.org/10.1126/science.aeb9953.

3. C. Tian, A. Sun, J. Chen, et al., "Photostable Donor–Acceptor Interface for Minimizing Energy Loss in Inverted Perovskite Solar Cells," *Nature Photonics* 20 (2026): 287–295, https://doi.org/10.1038/s41566-025-01827-6.

4. L. Zhan, Z. Sun, S. Zhang, et al., "UV and Thermally Stable Hole-Selective Contacts With Enhanced Assembly Density for Inverted Perovskite Solar Cells," *Nature Materials* 25 (2026): 1802–1810.

5. Y. Yang, S. Cheng, X. Yang, et al., "Hafnium Oxide Interface Stabilization for Efficient, Photothermally Stable Perovskite Solar Cells," *Science* 391 (2026): 926–930, https://doi.org/10.1126/science.aea3339.

6. Q. Cao, T. Wang, X. Pu, et al., "Co-Self-Assembled Monolayers Modified NiO_x for Stable Inverted Perovskite Solar Cells," *Advanced Materials* 36 (2024): 2311970, https://doi.org/10.1002/adma.202311970.

7. W. Wu, H. Gao, L. Jia, et al., "Stable and Uniform Self-Assembled Organic Diradical Molecules for Perovskite Photovoltaics," *Science* 389 (2025): 195–199, https://doi.org/10.1126/science.adv4551.

8. Z. Liu, D. He, Z. Zhang, et al., "High-Quality NiO_x Nanoparticles Synthesized via Low Temperature Chemical Precipitation Method for High-Performance Inverted Perovskite Photovoltaics," *Nature Communications* 17 (2026): 6993, https://doi.org/10.1038/s41467-026-73911-6.

9. J. Wang, Y. Yan, C. Wang, et al., "Redox-Mediated Stabilization of the Hole Transport Layer and Buried Interface Toward Stable Perovskite Solar Cells," *Angewandte Chemie International Edition* 65 (2026): e4012708, https://doi.org/10.1002/anie.4012708.

10. G. Qu, S. Cai, Y. Qiao, et al., "Conjugated Linker-Boosted Self-Assembled Monolayer Molecule for Inverted Perovskite Solar Cells," *Joule* 8 (2024): 2123–2134, https://doi.org/10.1016/j.joule.2024.05.005.

11. Y. Wang, Y. Feng, H. Yang, et al., "Covalent Tridentate Molecule Anchoring Enhances Nickel Oxide for Efficient Perovskite Solar Cells," *Advanced Materials* 37 (2025): e07730, https://doi.org/10.1002/adma.202507730.

12. D. Wang, Z. Liu, Y. Qiao, et al., "Rigid Molecules Anchoring on NiO_x Enable >26% Efficiency Perovskite Solar Cells," *Joule* 9 (2025): 101815, https://doi.org/10.1016/j.joule.2024.101815.

13. H. Chen, Q. Cao, X. Pu, et al., "Strong Coupling of NiO_x and Self-Assembled Molecules via Inserted Reductant for High-Performance Inverted Perovskite Solar Cells," *Advanced Materials* 37 (2025): e10553, https://doi.org/10.1002/adma.202510553.

14. C. Xie, D. N. Minh, R. Kret, et al., "Electrochemical Quantification of Phosphonic Acid Passivated Surface Sites of NiO_x for Perovskite Solar Cells," *Energy & Environmental Science* 19 (2026): 884–895, https://doi.org/10.1039/D5EE05065K.

15. J. Chen, X. Wang, T. Wang, et al., "Determining the Bonding–Degradation Trade-Off at Heterointerfaces for Increased Efficiency and Stability of Perovskite Solar Cells," *Nature Energy* 10 (2025): 181–190.

16. C. Fei, Y. Zhang, M. Wang, et al., "Limiting Phosphonic Acid Interlayer–Perovskite Reactivity to Stabilize Perovskite Solar Modules," *Science* 391 (2026): eadz7969, https://doi.org/10.1126/science.adz7969.

17. P. Wang, R. Sun, X. Sun, et al., "Electrostatically Enhanced Self-Assembled Monolayers Anchoring for Scalable and Stable Inverted Perovskite Solar Cells," *Advanced Materials* 38 (2026): e14735, https://doi.org/10.1002/adma.202514735.

18. J. Wang, B. Jiao, R. Tian, et al., "Less-Acidic Boric Acid-Functionalized Self-Assembled Monolayer for Mitigating NiO_x Corrosion for Efficient All-Perovskite Tandem Solar Cells," *Nature Communications* 16 (2025): 4148, https://doi.org/10.1038/s41467-025-59515-6.

19. Z. Qin, M. Chen, Z. Zhang, Y. Wang, and L. Han, "Inhibition of Interface Redox Reactions through Co-Self-Assembled Monolayers for Efficient and Stable Inverted Perovskite Solar Cells," *Advanced Functional Materials* 36 (2026): e20811.

20. M. Yuan, Y. Wang, Z. Liu, et al., "Redox-Improved Self-Assembled Monolayers for Inverted Perovskite Solar Cells," *Nature Communications* 16 (2025): 11330, https://doi.org/10.1038/s41467-025-66421-4.

21. C. Peng, X. Sun, B. Zhang, et al., "Strengthened Perovskite/SAM Heterointerface for Stable Perovskite Solar Cells," *Journal of the American Chemical Society* 147 (2025): 48391–48399, https://doi.org/10.1021/jacs.5c20051.

22. J. Zhang, Y. Li, L. Huo, et al., "Area-Selective Atomic Layer Deposition of AlO_X at the Buried Interface for High-Performance Perovskite Solar Cells," *Angewandte Chemie International Edition* 138 (2026): e16537, https://doi.org/10.1002/ange.202516537.

23. B. Li, C. Zhang, D. Gao, et al., "Suppressing Oxidation at Perovskite–NiO_x Interface for Efficient and Stable Tin Perovskite Solar Cells," *Advanced Materials* 36 (2024): 2309768, https://doi.org/10.1002/adma.202309768.

24. S. Qu, F. Yang, H. Huang, et al., "Redox Mediator-Modified Self-Assembled Monolayer Stabilizes a Buried Interface in Efficient Inverted Perovskite Solar Cells," *Energy & Environmental Science* 18 (2025): 3186–3195, https://doi.org/10.1039/D4EE05319B.

25. T. Li, W. Jiang, T. Wang, et al., "Quasi-Random Oriented Molecular Contacts for Inverted Perovskite Solar Cells With Improved Efficiency," *Nature Energy* 11 (2026): 866–875, https://doi.org/10.1038/s41560-026-02024-7.

26. F. Cao, S. Zhan, X. Dai, et al., "Redox-Sensitive NiO_x Stabilizing Perovskite Films for High-Performance Photovoltaics," *Journal of the American Chemical Society* 146 (2024): 11782–11791, https://doi.org/10.1021/jacs.4c00110.

27. C. Ge, H. Zhang, S. Chang, et al., "Stabilizing Sputtered NiO_x via In Situ Dissociative Adsorption Passivation for Efficient Perovskite Solar Cells," *Advanced Materials* 38 (2026): e73382, https://doi.org/10.1002/adma.73382.

28. P. Thai, B. L. Frey, R. F. Lalisse, et al., "Multisite Proton-Coupled Electron Transfer Enables Iodanyl Radical Catalysis," *Journal of the American Chemical Society* 147 (2025): 44336–44345, https://doi.org/10.1021/jacs.5c14648.

29. X. Zhang, Y. Li, P. Guo, et al., "Theory on Optimizing the Activity of Electrocatalytic Proton Coupled Electron Transfer Reactions," *Journal of Catalysis* 376 (2019): 17–24, https://doi.org/10.1016/j.jcat.2019.06.037.

30. J. Xiang, Q. Zhang, Y. Dou, D. Li, K. Deng, and L. Li, "Cost-Optimized Perovskite Solar Cells Enabled by Molecularly Engineered Hole Transport," *ACS Applied Materials & Interfaces* 18 (2026): 12670–12680, https://doi.org/10.1021/acsami.5c23142.

31. X. Yang, Y. Ni, Y. Zhang, et al., "Multiple-Defect Management for Efficient Perovskite Photovoltaics," *ACS Energy Letters* 6 (2021): 2404–2412, https://doi.org/10.1021/acsenergylett.1c01039.

15213773, 0, Downloaded from https://onlinelibrary.wiley.com/doi/10.1002/anie.202526576 by North China Electric Power University Beijing, Wiley Online Library on [08/10/2026]. See the Terms and Conditions (https://onlinelibrary.wiley.com/terms-and-conditions) on Wiley Online Library for rules of use; OA articles are governed by the applicable Creative Commons License

32. S. Yu, Z. Xiong, H. Zhou, et al., "Homogenized NiO_x Nanoparticles for Improved Hole Transport in Inverted Perovskite Solar Cells," *Science* 382 (2023): 1399–1404, https://doi.org/10.1126/science.adj8858.

33. Z. Lan, Y. Yang, H. Huang, et al., "Interfacial Electrostatic Repulsion Inhibits Iodide Ion Migration for Enhancing Reverse-Bias Stability of Perovskite Solar Cells," *Nature Communications* 16 (2025): 11407, https://doi.org/10.1038/s41467-025-66224-7.

34. Y. Zhang, Q. Song, G. Liu, et al., "Improved Fatigue Behaviour of Perovskite Solar Cells With an Interfacial Starch–Polyiodide Buffer Layer," *Nature Photonics* 17 (2023): 1066–1073, https://doi.org/10.1038/s41566-023-01287-w.

35. Y. Zhang, F. Pei, C. Zhu, et al., "Thermo-Mechanically Robust Inverted Perovskite Solar Cells Toward Extreme Environments," *Advanced Functional Materials* 36 (2026): e75697, https://doi.org/10.1002/adfm.75697.

36. T. Zhou, Y. Li, W. Zhao, Y. Chen, Y. Gao, and Y. Liu, "Multidentate Chelation Modulates PbI_2 Crystallization and Buried-Interface Formation in Perovskite Solar Cells," *Angewandte Chemie International Edition* 65 (2026): e3088935, https://doi.org/10.1002/anie.3088935.

Supporting Information

Additional supporting information can be found online in the Supporting Information section.

Supporting File: anie75162-sup-0001-SuppMat.docx.

15213773, 0, Downloaded from https://onlinelibrary.wiley.com/doi/10.1002/anie.202675 by North China Electric Power University Beijing, Wiley Online Library on [08/10/2026]. See the Terms and Conditions (https://onlinelibrary.wiley.com/terms-and-conditions) on Wiley Online Library for rules of use; OA articles are governed by the applicable Creative Commons License